THERMOPHYSICAL AND THERMOCHEMICAL PROPERTIES OF XENOTIME MINERAL-INSPIRED RARE EARTH PHOSPHATE ENVIRONMENTAL BARRIER COATINGS

Pádraigín Stack[1], William Riffe[1], Hunter Schonfeld[2], Patrick Hopkins[2], Elizabeth Opila[1]
1. Materials Science and Engineering, University of Virginia, United States
2. Mechanical and Aerospace Engineering, University of Virginia, United States

Abstract
Combustion engines operate more efficiently when operated at higher temperatures. However, this can rapidly degrade engineering materials; environmental barrier coatings (EBC) are used to protect hot section components. Current EBCs, rare earth (RE=La-Lu, Sc, Y) disilicates (REDS), withstand harsh engine environments showing low oxidation rates in high-temperature water vapor, but improvements can be made to their resistance to siliceous debris, such as dust and ash ingested by the engine. Motivation comes from the fact that rare earth containing minerals, like xenotime, are used in a hydrometallurgical separation process which requires strong acids and strong bases to extract the rare earth cations. The hydrometallurgical process takes the rare earths in the mineral as rare earth phosphates ($REPO_4$) and separates them into separate rare earth oxides RE_2O_3. This is an expensive, inefficient, and hazardous process which requires over sixty stages to separate two rare earth cations. Greener coatings could be made using the minerals with minimal processing. Preliminary work on $YbPO_4$ has demonstrated similar thermal expansion and high-temperature water vapor performances to the REDS while offering significantly better resistance to siliceous debris. Efficacy of $REPO_4$ coatings by studying thermal conductivity, thermal expansion, high-temperature water vapor resistance, and siliceous debris resistance is discussed.

1. Background
Higher efficiency in gas combustion engines is desired to reduce emissions. SiC-ceramic matrix composites (CMC) have been proposed as a replacement for Ni-based superalloys to reduce weight and increase maximum operating temperature. SiC slowly forms SiO_2 following parabolic growth rates in dry oxygen. High-temperature high-pressure water vapor is produced by the engine results in volatilization of the SiO_2[1–3]. These degradative processes can be reduced by an environmental barrier coating (EBC) which primarily acts as a sacrificial layer. The main goal of an EBC for passenger aircraft is to prevent water vapor and contaminants such as calcium-magnesium-alumino silicates (CMAS) from interacting with the substrate. EBCs need to have low reactivity with steam and CMAS. Compatibility of the EBC and the substrate must be considered for material selection. Phase instability of the EBC and differences in coefficient of thermal expansion (CTE) will result in the generation of stresses during thermal cycling leading to the formation of cracks allowing for fast diffusion paths and spallation. Low thermal conductivity would also grant the properties of a thermal barrier coating, where the system could operate at higher temperatures for longer and further reduce the kinetic rates.

The current generation of EBCs are rare earth (RE=La-Lu, Sc, Y) disilicates (DS or REDS) on SiC-CMCs with a Si bond coat. REDS have a similar CTE to SiC-CMC, but the monoclinic symmetry leads to stress generation due to anisotropic expansion. Molten CMAS can rapidly penetrate REDS resulting in interaction with the substrate. REDS react with water vapor to volatilize a silica group forming RE monosilicates (REMS). REMS experience slower reaction kinetics with steam but produce large thermal

stresses due to phase transformation and a CTE mismatch. Depending on the RE cation, REMS can form dense, protective apatite layers which prevent the ingress of CMAS.

There is a continued interest in improving the properties of EBCs. The RE used for the REDS can be found in minerals such as xenotime and monazite in the form of $REPO_4$. The large RE cations (RE=LA-Tb) are found in monazite while xenotime contains the smaller RE cations (RE=Y, Sc, Tb-Lu). The minerals are thermodynamically stable and are mined and separated into individual RE_2O_3. This process requires the repetitive use of strong acids and bases and can involve over 65 stages for the extraction process[4]. The viability of $REPO_4$ using xenotime minerals as a lithomimetic inspiration is studied in the current report.

2. Methods

a. Characterization and Synthesis of $REPO_4$

Multiple xenotime minerals are gathered from around the world. The samples are mounted and polished and the composition is approximated using energy dispersive spectroscopy (EDS). The results for these observations are summarized in Table 1. From this, it is concluded that the average composition of xenotime minerals is $(Y_{0.08}Gd_{0.04}Dy_{0.07}Er_{0.05}Yb_{0.04})PO_4$. There are five RE cations in a high-entropy mixture.

	RE (%)	Y	Gd	Dy	Er	Yb
BRA	22	0.79	0.05	0.09	0.04	0.02
COD	22.7	0.79	0.04	0.08	0.05	0.05
NOR	18.1	0.81	0.04	0.07	0.04	0.04
PAK	23.4	0.80	0.04	0.08	0.05	0.03
Mean	-	0.80	0.04	0.08	0.05	0.04
Model	**-**	**0.8**	**0.04**	**0.07**	**0.05**	**0.04**

Table 1 Summary of composition of rare earth elements in xenotime minerals from throughout the world determined by energy dispersive spectroscopy.

The $REPO_4$ of interest are synthesized using a co-precipitation method using RE_2O_3 and H_3PO_4 in H_2O following the reaction:

$$RE_2O_3 + 2H_3PO_4 = 2REPO_4 + 3H_2O \quad (1)$$

The resulting $REPO_4$ are hydrated, so the product is calcined at 1100°C for 24h. The product is milled to a fine powder and the composition is confirmed using X-ray Diffraction (XRD). Phase purity of synthesized powder is demonstrated in Figure 1. Except for $GdPO_4$, which is expected to be monoclinic, the $REPO_4$ are all tetragonal with peaks close to each other. The peak list of the single component $REPO_4$ matches those found in literature and the peaks are narrow so the multicomponents are assumed to also be well mixed within the crystal structure.

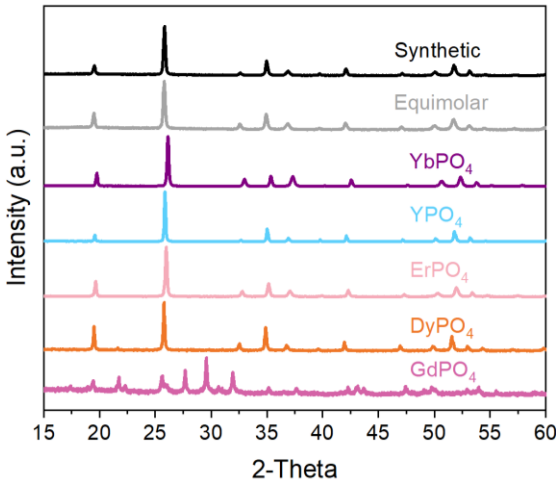

Figure 1 XRD data of synthesized $REPO_4$ powder demonstrating phase purity and similar response.

b. Thermophysical properties of $REPO_4$

Coefficient of thermal expansion is characterized using hot-stage powder diffraction. The diffractometer is outfitted with a rotating hot-stage which is programed to take measurements from 25-1200°C at 50°C intervals. XRD response data is set against LaB_6 and processed using the sequential Rietveld refinement in GSAS-II[5].

$REPO_4$ is densified using spark plasma sintering (SPS) with a 1500°C 65 MPa hold for 30 minutes. Densified pucks are baked out at 1500°C in a box furnace for 30h. Samples are polished to 0.02 nm and coated with an Al transducer. Time Domain-Thermal Reflectance (TDTR) was used to calculate the thermal conductivity of the $REPO_4$ species. As TDTR is a non-destructive method, it is also performed on a real xenotime mineral. Measurements are taken at room temperature using a Ti:Sapphire source.

c. CMAS resistance properties of $REPO_4$

Samples are produced from powder using the previously described densification method. Samples are cut from disks into 10 mm x 10 mm x 3 mm coupons and polished to 1 µm.

CMAS pellets are comprised of a composition described by Kramer, et al[6], $33CaO\text{-}9MgO\text{-}13AlO_{1.5}\text{-}45SiO_2$ (UCSB). Crushed glass powder is pressed into a pellet with a mass of 40mg using a hydraulic press and is sintered at 1100°C for 6h.

Pellets are placed on the polished coupon to obtain a CMAS loading of 40 mg/cm^2, which will allow for the comparison of $REPO_4$ with other material classes[7,8]. The sample is loaded into a box furnace to be exposed to 1300°C lab air with three separate exposure times of 4, 24, and 96h. The heating and cooling rate was controlled at 5°C/min. After exposure, coupons are characterized with XRD to observe any crystalline reaction products. Plan view scanning electron microscope (SEM) micrographs are taken and stitched together to allow for observations of CMAS melt pool dimensions.

d. Steam resistance of $REPO_4$

Densified coupons are prepared following the same process for CMAS testing. Samples are placed onto a Pt foil lined alumina boat and vertically secured with Pt wire at a yaw of 45°. The boat is loaded into a horizontal tube furnace with flowing Ar and placed 1 mm from a Pt capillary. The furnace is heated to 1400°C and 100% water vapor from the capillary impinges the sample and creates a gas flow speed gradient range from 250-100 m/s.[9] This emulates the high-temperature, high-pressure water vapor product from combustion. Samples are exposed for 72, 120, and 240h. Exposed coupons are characterized with XRD to evaluate reaction product. Plan view SEM micrographs are taken to construct a map of the surface to characterize vapor flow and observe surface changes. Samples are then cross sectioned to measure reaction product thickness using SOFIA, an open-source tool for measuring thickness of reaction products[10–12].

3. Results

a. Thermophysical properties

Mineral-synthetic $REPO_4$ powder volumetric CTE, Figure 2, demonstrates a range of 4.5-$6x10^{-6}$ $°C^{-1}$ between 25 and 1200°C. This value falls outside the range for SiC indicating that stresses will be generated at the interface between the materials. From the volumetric CTE of other $REPO_4$ species, Figure 3, the trend lines for all tetragonal $REPO_4$ species share similar ranges. There is a noticeable exception for $GdPO_4$, but this is a monoclinic structure which may explain the difference. Additionally, the inclusion of $GdPO_4$ in the multicomponent $REPO_4$ does not seem to significantly increase CTE values.

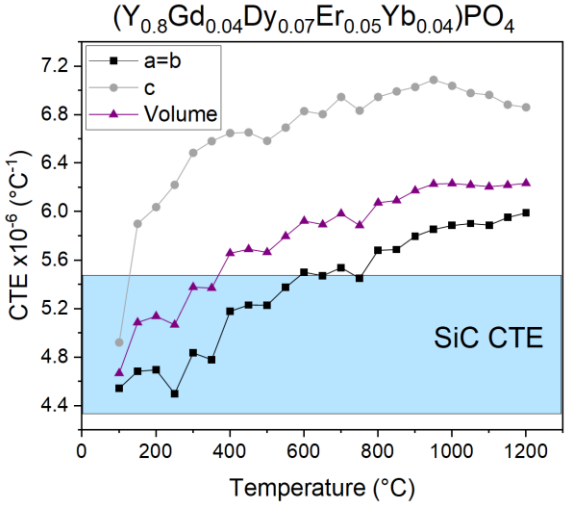

Figure 2 Powder hot-stage XRD thermal expansion data for mineral-synthetic xenotime $REPO_4$.

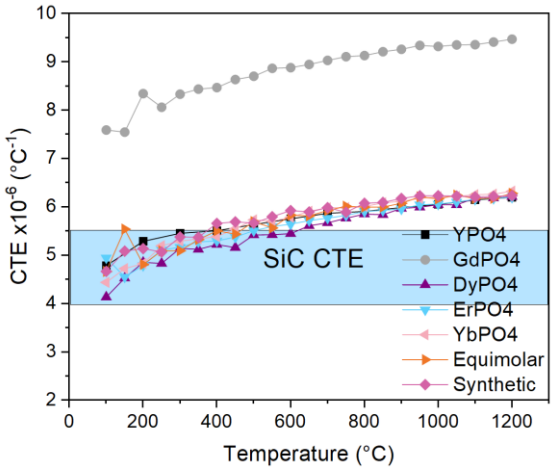

Figure 3 Powder hot-stage XRD volumetric thermal expansion data for multiple $REPO_4$ species.

TDTR results for xenotime mineral and densified $REPO_4$ species are listed in Table 2. Single component tetragonal $REPO_4$ are located between 6-14 $Wm^{-1}K^{-1}$ which is larger than the reported value for YbDS. However, multicomponent samples and xenotime mineral demonstrate a reduction in thermal conductivity from rule of mixture.

Composition	Crystal Symmetry	Thermal Conductivity ($Wm^{-1}K^{-1}$)
Mineral	Tetragonal	3.4 +/- 0.40
$GdPO_4$	Monoclinic	4.2 +/- 0.64
Equimolar	Tetragonal	4.9 +/- 0.80
YbDS	Monoclinic	5.84
$YbPO_4$	Tetragonal	6.5 +/- 1.13
Synthetic	Tetragonal	6.7 +/- 0.87
$DyPO_4$	Tetragonal	8.3 +/- 1.23
$ErPO_4$	Tetragonal	11.2 +/- 1.58
YPO_4	Tetragonal	14.0 +/- 2.94

Table 2 Single point thermal conductivity values for xenotime mineral and $REPO_4$ species using room temperature TDTR.

A thermal conductivity map of the xenotime mineral is show in Figure 4. The mineral shows a range of thermal conductivities and regions in black where there were pores or other artifacts. Most of the map of the sample is closer to the mineral-synthetic value listed in Table 2.

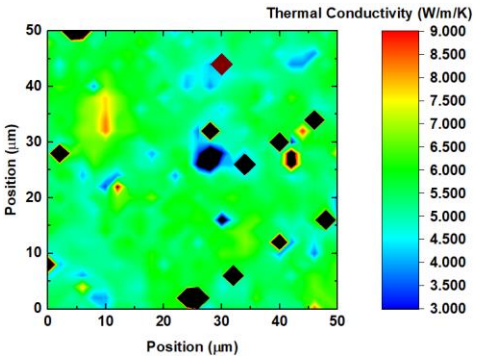

Figure 4 Thermal conductivity map of xenotime mineral from room temperature TDTR.

b. CMAS Reaction

YPO_4, $ErPO_4$, $YbPO_4$, and the multicomponent $REPO_4$ are exposed to 40mg/cm^2 loading of UCSB CMAS in 1300°C lab air for 4, 24, and 96h. Figure 5-7 depicts cross sectional micrographs located toward the center of the sample of all time exposures for $ErPO_4$, mineral-synthetic, and equimolar compositions. In all micrographs, a reaction product layer is seen in the middle of the micrograph and appears to smooth out as the time increases. Additionally, the residual CMAS is only seen in the 4h micrograph and the porosity of the $REPO_4$ increases with exposure time.

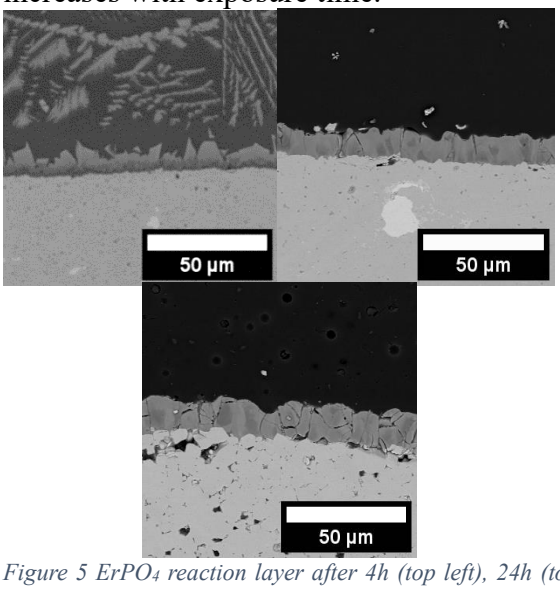

Figure 5 $ErPO_4$ reaction layer after 4h (top left), 24h (top right), and 96h (bottom) exposure to 1300°C lab air with 40 mg/cm^2 UCSB loading.

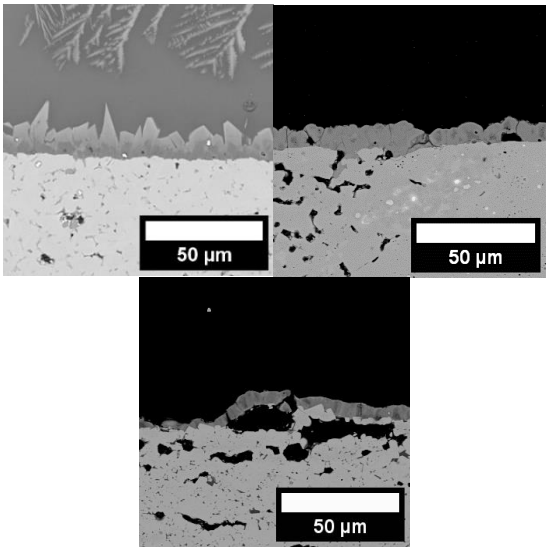

Figure 6 mineral-synthetic reaction layer after 4h (top left), 24h (top right), and 96h (bottom) exposure to 1300°C lab air with 40 mg/cm² UCSB loading,

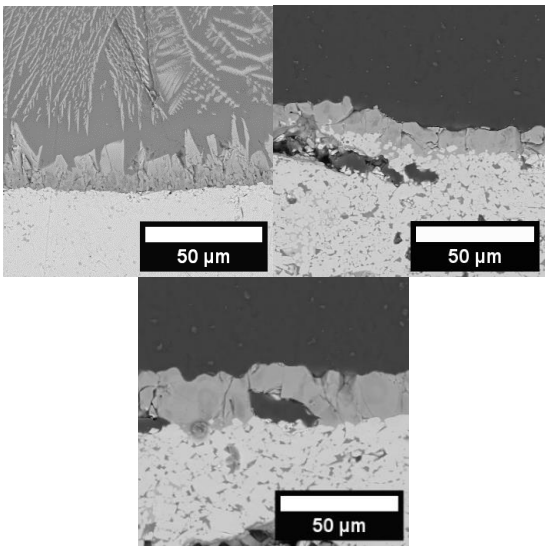

Figure 7 Equimolar reaction layer after 4h (top left), 24h (top right), and 96h (bottom) exposure to 1300°C lab air with 40 mg/cm² UCSB loading.

$YbPO_4$ was reported in a previous study by Ridley, et al[8]. Overall reaction product thicknesses are measured and reported with the other $REPO_4$ species in Figure 8. A parabolic growth rate was determined for $YbPO_4$ and is seen in the other compositions.

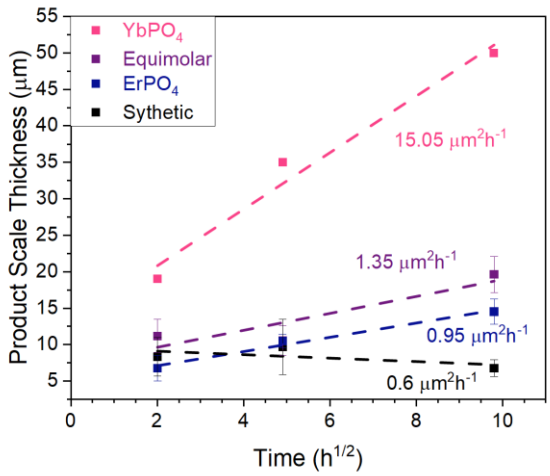

Figure 8 Reaction product thickness as a function of square root time for $REPO_4$ exposed to 1300°C air with 40 mg/cm² UCSB CMAS loading.

The relative concentration of RE in reaction product layer of the mineral-synthetic $REPO_4$ is quantized using EDS and is summarized in Figure 9 and Table 3. Y appears in smaller concentrations than the base material and results in greater concentrations of Gd and Dy.

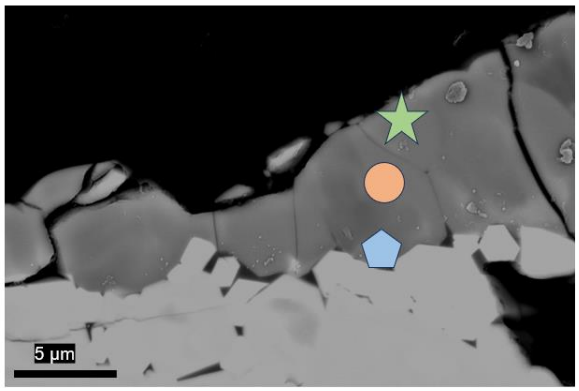

Figure 9 Mineral-synthetic reaction product layer after 96 h 1300°C air with 40 mg loading of UCSB CMAS

	Relative Ratio of RE in Product				
	Y	Gd	Er	Dy	Yb
★	0.72	0.09	0.06	0.12	0.02
●	0.72	0.09	0.06	0.11	0.02
⬟	0.71	0.07	0.07	0.12	0.03
Base	0.8	0.04	0.07	0.05	0.04

Table 3 Summary of relative composition of rare earth elements in CMAS reaction product layer in Figure 9.

c. Steam resistance of $REPO_4$

YPO_4, $DyPO_4$, and $YbPO_4$ have been exposed to 1400°C water vapor for 72, 120, and 240h. Sample cross section micrograph of $DyPO_4$ 240h is found in Figure 10.

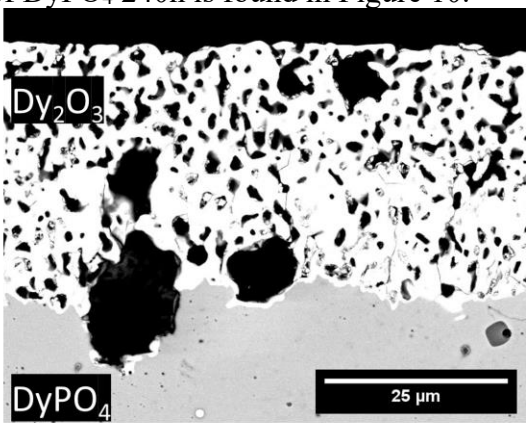

Figure 10 Cross sectional micrograph of $DyPO_4$ exposed to 1400°C water vapor for 240h.

Steam reaction products for the $REPO_4$ are characterized by XRD and EDS and determined to be RE_2O_3. The total thickness of the RE_2O_3 is measured using several micrographs located at and around the high-velocity region. The median thickness values are reported in Figure 11 and are determined to follow a parabolic growth rate. The $REPO_4$ are plotted against the conventional EBC material, YbDS[13]. A lower parabolic growth rate is seen for all tested $REPO_4$.

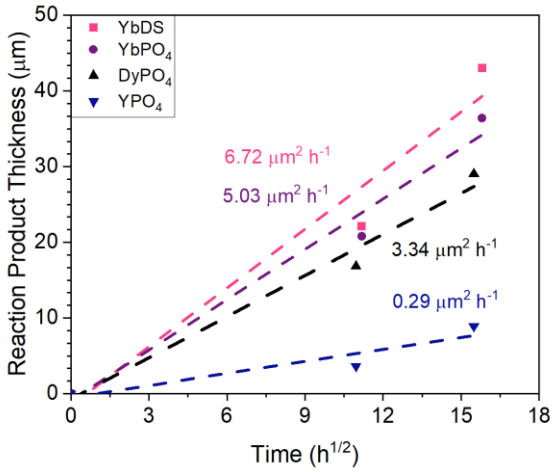

Figure 11 Summary of reaction product thickness as a function of square root time for $REPO_4$ exposed to 100% water vapor at 1400°C.

4. Discussion

CTE measurements of the $REPO_4$ species indicate that there will be stress generations due to thermal cycling. The difference between the ranges is not large but may become detrimental at temperatures higher than could be measured with the equipment. The differences could result in spallation of the coating or cracks which will act as short circuit diffusion paths.

Thermal conductivity of the $REPO_4$ is not favorable, $REPO_4$ cannot be used solely as a thermal barrier coating (TBC). Ideally, a TBC would have a value of less than 1 $Wm^{-1}K^{-1}$. If a thermal barrier coating is desired, it would be recommended to use thermal barrier coatings such as YSZ in a multilayer system. However, RE_2O_3 do demonstrate the ability to act as a TBC and as this is a reaction product that occurs during exposure to high-temperature water vapor, a TBC may not be required. Although the system appears porous in the micrographs, it still follows parabolic growth rates indicating that it is a diffusion inhibitor. Also, it demonstrates lower kinetic rates than the YbDS. However, additional studies need to be performed on the thermal cycling capabilities of RE_2O_3 and $REPO_4$. Study into the phosphorous vapor reaction products needs to be investigated as

phase diagrams would indicate that there are multiple stable intermediate phases between $REPO_4$ and RE_2O_3.

CMAS interactions with $REPO_4$ are not well understood. The lack of residual CMAS at longer exposure times indicates that there is CMAS infiltration. The $REPO_4$ does not form massive blisters as rapidly as YbDS and indicates the formation of an apatite-like reaction product that may inhibit CMAS infiltration. There seems to be a breakdown process occurring allowing for CMAS infiltration. Reaction product breakdown and CMAS infiltration needs to be further investigated. Coupon recession measurements and different CMAS loadings may help characterize this process.

5. Summary

Phase pure single and multicomponent $REPO_4$ species can be synthesized using RE_2O_3 and H_3PO_4. CTE is determined using hot stage powder diffraction. The identified range is slightly higher than that of SiC which the coating might be adhered to. TDTR indicates that $REPO_4$ species would not be suitable as thermal barrier coatings and an additional coating would be required to obtain these properties. Preliminary results show an improvement compared to REDS through the formation of a reaction product which may lead to delayed CMAS penetration. However, only $YbPO_4$ has demonstrated no CMAS penetration[8]. Steam reactivity of $REPO_4$ follows a parabolic trend indicating diffusion-controlled mechanisms. The $REPO_4$ show a smaller rate constant than YbDS which is favorable. Additional study of the CMAS and steam resistance of the $REPO_4$ need to be studied. This can include but is not limited to different CMAS loadings and steam exposure temperatures.

Acknowledgements

Thank you to Dr. Daniel Cole, program manager at the US Army Research Office for providing funding for this project; ARO Cooperative Agreement Number W911NF-22-2-0022. Additional thanks to the Virginia Space Grant Consortium for project funding.

References

1. Meschter, P. J., Opila, E. J. & Jacobson, N. S. Water vapor-mediated volatilization of high-temperature materials. *Annu Rev Mater Res* **43**, 559–588 (2013).
2. Jacobson, N. S., Opila, E. J., Myers, D. L. & Copland, E. H. Thermodynamics of gas phase species in the Si-O-H system. *Journal of Chemical Thermodynamics* **37**, 1130–1137 (2005).
3. Opila, E. J. & Hann, R. E. Paralinear oxidation of CVD SiC in water vapor. *Journal of the American Ceramic Society* **80**, 197–205 (1997).
4. Quinn, James. E., Soldenhoff, K. & Stevens, G. W. Alternatives to 2-Ethylhexyl Phosphonic Acid, Mono-2-Ethylhexyl Ester for the Separation of Rare Earths. in *The Minerals, Metals & Materials Society* 2765–2775 (Springer International Publishing, 2018). doi:10.1007/978-3-319-95022-8_234.
5. Toby, B. H. & Von Dreele, R. B. GSAS-II: the genesis of a modern open-source all purpose crystallography software package. *urn:issn:0021-8898* **46**, 544–549 (2013).
6. Krämer, S., Yang, J., Levi, C. G. & Johnson, C. A. Thermochemical Interaction of Thermal Barrier Coatings with Molten CaO–MgO–Al2O3–SiO2 (CMAS) Deposits. *Journal of the American Ceramic Society* **89**, 3167–3175 (2006).
7. Webster, R. I. & Opila, E. J. Mixed phase ytterbium silicate environmental-barrier coating

materials for improved calcium–magnesium–alumino-silicate resistance. *J Mater Res* **35**, 2358–2372 (2020).
8. Ridley, M., McFarland, B., Miller, C. & Opila, E. YbPO4: A novel environmental barrier coating candidate with superior thermochemical stability. *Materialia (Oxf)* **21**, 101289 (2022).
9. Ridley, M. & Opila, E. Thermochemical stability and microstructural evolution of Yb2Si2O7 in high-velocity high-temperature water vapor. *J Eur Ceram Soc* **41**, 3141–3149 (2021).
10. Stack, P. *et al.* Dry air cyclic oxidation of mixed Y/Yb disilicate environmental barrier coatings and bare silica formers. *J Eur Ceram Soc* **42**, 3345–3350 (2022).
11. Kane, K. *et al.* Oxidation of 3D-printed SiC in air and steam environments. *Journal of the American Ceramic Society* **104**, 2225–2237 (2021).
12. Kane, K. *et al.* Evaluating steam oxidation kinetics of environmental barrier coatings. *Journal of the American Ceramic Society* **105**, 590–605 (2022).
13. Ridley, M. & Opila, E. Variable thermochemical stability of RE2Si2O7 (RE = Sc, Nd, Er, Yb, or Lu) in high-temperature high-velocity steam. *Journal of the American Ceramic Society* **105**, 1330–1342 (2022).